Engineering Analysis with Boundary Elements 143 (2022) 293–304

Contents lists available at ScienceDirect

Engineering Analysis with Boundary Elements

journal homepage: www.elsevier.com/locate/enganabound

2.5D singular boundary method for exterior acoustic radiation and scattering problems

Javad Fakhraei [a,*], Robert Arcos [a,b,*], Teresa Pàmies [a], Jordi Romeu [a]

[a] Acoustical and Mechanical Engineering Laboratory (LEAM), Universitat Politècnica de Catalunya (UPC), Carrer Colom, 11, 08222 Terrassa (Barcelona), Spain
[b] Serra Húnter Fellow, Universitat Politècnica de Catalunya (UPC), Spain

ARTICLE INFO

Keywords:
2.5D singular boundary method
2.5D method of fundamental solutions
2.5D boundary element method
Acoustic radiation and scattering

ABSTRACT

In this paper, a numerical methodology based on a two-and-a-half-dimensional (2.5D) singular boundary method (SBM) to deal with acoustic radiation and scattering problems in the context of longitudinally invariant structures is proposed and studied. In the proposed 2.5D SBM, the desingularisation provided by the subtracting and adding-back technique is used to determine the origin intensity factors (OIFs). These OIFs are derived by means of the OIFs of the Laplace equation. The feasibility, validity and accuracy of the proposed method are demonstrated for three acoustic benchmark problems, in which detailed comparisons with analytical solutions, the 2.5D boundary element method (BEM) and the 2.5D method of fundamental solutions (MFS) are performed. As a novelty of the present study, it is found that the 2.5D SBM provides a higher numerical accuracy than the 2.5D linear-element BEM and lower than the 2.5D quadratic-element BEM. Although the results obtained depict that a nodal approximation of the boundary geometry leads to a significant reduction in the accuracy of the 2.5D SBM, the delivered errors are still acceptable. For complex geometries, the 2.5D SBM is found to be simpler and more robust than the 2.5D MFS, since no optimization procedure is required.

1. Introduction

Problems related to acoustic waves propagation in unbounded domains are frequently encountered in many engineering applications. The domain-type discretization methods, such as the finite element method (FEM), are not efficient when dealing with this kind of problems, since they require a massive domain meshing, especially at high frequencies, which is often computationally costly [1]. As an alternative approach, the boundary element method (BEM) is found to be more efficient for unbounded domain problems, since its boundary-oriented modelling inherently allows for an efficient treatment of such domains [2]. However, despite the fact that the BEM only requires a mesh of the boundary instead of the full domain, it involves an intricate mathematical formulation together with some numerical issues, such as regularization procedures to deal with the singularities arisen from the fundamental solutions, fully populated system matrices and troublesome surface meshing in 3D complex domains. Leaving the complex formulae aside, these circumstances result in an increase on computational time and memory requirements, which is probably the main drawback of the BEM. Due to these disadvantages, a new generation of boundary-type meshless numerical methods that require neither domain nor boundary meshing have been developed in last two decades. Among meshless methods, the method of fundamental solutions (MFS) has been extensively applied to solve a variety of acoustic problems thanks to its merits on being mathematically simple, easy-to-program, and automatically satisfying the Sommerfeld radiation condition at infinity. Two of the earliest works regarding the application of the MFS to acoustic problems were presented by Shippy and Kondapalli [3,4]. Later, Karageorghis [5] used the MFS with fixed sources for the solution of Helmholtz eigenvalue problems. Fairweather et al. [6] reviewed the previous developments of the MFS for scattering and radiation problems in fluids and solids, establishing a general benchmark for its application. Marin [7] investigated the combination of the MFS and the singularity subtraction technique (SST) for problems associated with the modified Helmholtz equations in two-dimensional (2D) domains containing edge cracks and V-notches. Karageorghis et al. [8] employed the MFS for detecting a sound-soft scatterer surrounding a host acoustic homogeneous medium due to a given point source inside it. Qu et al. [9] applied the localized MFS (LMFS) to solve the 2D interior Helmholtz equation at high frequencies. The presented numerical examples showed that the LMFS has a lower computational complexity than the traditional MFS and it can be used for simulating large-scale acoustic problems with complicated geometries. The application of the MFS to predict the acoustic insulation performance of a T-shaped thin barrier in the presence of a point source was reported in [10]. However,

* Corresponding authors.
E-mail addresses: javad.fakhraei@upc.edu (J. Fakhraei), robert.arcos@upc.edu (R. Arcos).

https://doi.org/10.1016/j.enganabound.2022.06.017
Received 17 September 2021; Received in revised form 7 May 2022; Accepted 22 June 2022
Available online 4 July 2022

although significant amount of research has been carried out to enhance the MFS capabilities, the method still has a serious disadvantage: the determination of the optimal fictitious boundary, especially for complicated boundary geometries, restrains the MFS applications to real engineering problems. Several modification schemes have been devised to solve this drawback by investigating approaches where the virtual sources can be placed directly on the physical boundary. Some of these methods include the boundary collocation method (BCM) [11], the boundary knot method (BKM) [12], the localized boundary knot method (LBKM) [13,14], the singular meshless method (SMM) [15], the regularized meshless method (RMM) [16] and the singular boundary method (SBM) [17], to name just a few.

The SBM was firstly presented by Chen and Wang [17]. Recently, this method has appeared to be an effective alternative to overcome some drawbacks of the other techniques, like the limited applicability, low accuracy and ill-conditioning problems. In the following, some studies of the method applicability for acoustics analysis are listed. Lin et al. [18] investigated the SBM when dealing with acoustic problems including singular boundary conditions by combining the SBM with the SST. Fu et al. [19] proposed the improved singular boundary method (ISBM) for acoustic radiation and scattering, which is a combination of the classical SBM with the Burton and Miller's formulation. Numerical results demonstrate that this modification scheme enhances the quality of the solution in the vicinity of the corresponding interior eigenfrequencies. Fu et al. [20] applied the SBM for solving water wave-structure interaction and SH wave scattering problems. Qu et al. [21] applied a fast multipole accelerated SBM for the 3D Helmholtz equation in low-frequency regimes. In another study, Qu et al. [22] introduced a diagonal form of the fast multipole SBM to overcome the high computational requirements of the SBM interpolation matrix for high-frequency acoustic radiation and scattering problems. To reduce the high computational requirements of the SBM in 3D problems, Li [23] presented a fast SBM to solve 3D Helmholtz equations that employs the pre-corrected fast Fourier transform (PFFT) to accelerate the SBM numerical process. The results showed that the PFFT-SBM has an advantage over the standard SBM in terms of memory and CPU time. Fu et al. [24] developed the SBM in conjunction with the fast Toeplitz-type matrix solvers (FTMS) for acoustic wave propagation analysis at low and moderate frequencies in periodic structures. The numerical results demonstrated that by employing this method, the computational time and storage requirements are significantly reduced with respect to traditional SBM routines. Recently, Wang et al. [25] proposed the localized singular boundary method (LSBM) to solve the Laplace and Helmholtz equations in 2D arbitrary domains. Compared with the traditional SBM, the proposed LSBM can effectively avoid the boundary layer effect (appearing for field points located close to the boundary) and requires less memory storage and computational effort because the produced interpolation system matrices are sparse and banded. Typically, the SBM utilizes the single-layer fundamental solutions as kernel functions and introduces the so-called origin intensity factors (OIFs) to circumvent the singularities of the fundamental solutions where the collocation and source points coincide. It approximates the solution of the problem with a linear combination of fundamental solutions of the governing equation of interest. The vital issue in the SBM is the determination of the OIFs, which can be calculated through empirical, analytical or numerical techniques. In the original SBM, the inverse interpolation technique (IIT) [17] was proposed to evaluate the OIFs by using sample solutions of the governing equation of the problem. Chen and Gu [26] introduced the desingularisation provided by the subtracting and adding-back technique to obtain a numerical-analytical formula so that the OIFs are determined directly without any sample solutions. Fu et al. [27] compared three methodologies for the OIFs determination on Neumann and Dirichlet boundaries in exterior wave propagation problems: the IIT; a semi-analytical technique that combines the subtracting and adding-back technique and the IIT; and a semi-analytical technique based on the integral mean value of the Laplace fundamental solution. Results show that semi-analytical solutions provided a higher numerical stability, being the second methodology the one showing the best accuracy. Li et al. [28] presented new explicit empirical formulas to determine the OIFs on Neumann and Dirichlet boundary conditions for 2D and 3D Laplace and Helmholtz equations. With these empirical formulas, the OIFs can be obtained using neither the subtracting and adding-back technique nor numerical integration. A strictly mathematical regularized approach for the evaluation of the OIFs for the 3D Helmholtz equation at high frequencies was provided in [29]. The novelty of the work is to propose two artificially constructed general solutions that can be used to directly evaluate the OIFs by using the subtracting and adding-back technique, which yields on a fully integration- and mesh-free technique. The numerical demonstrations show that the proposed OIF formulas can be successfully used to avoid the singularity and hyper singularity problems encountered in the application of the SBM or the BEM.

In some acoustic wave propagation analyses required in engineering applications, such as noise emission assessments for road and railway transportation systems, the computational domain can be assumed to be longitudinally invariant, meaning that the geometry of the system is considered to have a constant cross section along its longitudinal direction. The methodologies to solve these problems can be constructed in the framework of the two-and-a-half-dimensional (2.5D) domain. The 2.5D domain is reached by the application of the Fourier transform to the governing equations along the coordinate associated with the invariant direction. Then, the system can be solved in a 2D framework and the 3D solutions can be obtained by using the corresponding Fourier inverse transform. Thus, the advantage of this approach is the reduction of the problem dimensionality by one, which results in strong reduction of the computational costs and memory requirements in the context of mesh-based approaches [30]. Regarding this benefit, the computational efficiency can be further enhanced if meshless methods are employed when dealing with unbounded domain problems. Methodologies based on the 2.5D formulation are being used nowadays to model engineering acoustic problems. Sheng and Zhong [31] proposed a 2.5D acoustic BEM to simulate the sound radiation of high-speed railway slab tracks subjected to a moving harmonic load. A similar model has been used recently by Li et al. [32] to simulate the noise transmission from the wheels, rails and sleepers to the external surfaces of a train, and by Deng et al. [33] to study the noise insulation capabilities of poro-elastic panels. Ghangale et al. [34] presented a combined methodology based on the 2.5D structural FEM-BEM and the 2.5D acoustic BEM for the prediction of re-radiated noise in underground simple tunnels. Also, some studies have employed 2.5D meshless methodologies to analyse engineering acoustic problems. In this regard, the potential applications of the 2.5D MFS for the prediction of re-radiated noise in railway traffic systems were discussed in [34,35]. Recently, the 2.5D SBM [36] has been preliminarily proposed and tested for acoustic problems excited by harmonic point sources. The numerical results verified the effectiveness and accuracy of the proposed approach and reported a significant reduction of memory storage in comparison with the 3D acoustic SBM.

The objective of this paper is to propose and study, in a computational context, a 2.5D SBM approach to deal with acoustic wave propagation problems in where the geometry of the system is longitudinally constant. In the proposed 2.5D SBM, the desingularisation provided by the subtracting and adding-back technique is used to determine the OIFs. These OIFs are derived by means of the OIFs of the Laplace equation due to the same order of the singularities in the fundamental solutions of Laplace and Helmholtz equations. The feasibility, validity and accuracy of the proposed 2.5D SBM are investigated in the framework of three benchmark examples: the acoustic radiation and wave scattering problems for an infinite cylinder and the acoustic radiation of an infinite beam with a star-like cross section. In order to make a detailed assessment of the proposed approach, other methodologies are applied and then compared in terms of numerical

accuracy and computational efficiency. These alternative approaches are the 2.5D MFS and the 2.5D BEM considering linear and quadratic boundary elements (referred as 2.5D LE-BEM and 2.5D QE-BEM from now on). For the example associated to the infinite cylinder, the available analytical solution is used as a reference for the accuracy comparisons. Furthermore, the effect on the 2.5D SBM accuracy induced by considering the exact geometry of the boundary instead of the node-based approximation is also investigated in this study. After the present introduction, the rest of this paper is arranged as follows: Section 2 states the formulation of the proposed 2.5D acoustic SBM approach. Section 3 presents the verification and comparison of the different 2.5D acoustic numerical methods and discusses the discrepancies between them for the benchmark examples. Finally, some concluding remarks are presented in Section 4.

2. Mathematical formulation

In this section, the formulation of the proposed 2.5D SBM is presented. In a first instance, the acoustic problem is written in the 2.5D domain. Secondly, the proposed SBM is described in detail in the 2.5D context.

2.1. 2.5D formulation for acoustic problems

The problem under consideration is the propagation of acoustic waves in a 3D homogeneous isotropic medium Ω. In this problem the pressure field can be modeled in the frequency domain by the well-known Helmholtz equation

$$\left(\Delta + k^2\right) p(\mathbf{x}) = 0, \quad \mathbf{x} \in \Omega, \tag{1}$$

where Δ is the Laplacian operator, $p(\mathbf{x})$ represents the acoustic pressure at a generic point $\mathbf{x} = \{x, y, z\}^{\mathrm{T}}$ inside the domain, k is the acoustic wavenumber in a 3D context and it is equal to ω/c, ω is the angular frequency and c is the sound wave speed in the medium. Two kinds of boundary conditions are usually considered: the Dirichlet boundary condition

$$p(\mathbf{x}) = p_b(\mathbf{x}), \quad \mathbf{x} \in \Gamma, \tag{2}$$

or the Neumann boundary condition

$$v(\mathbf{x}) = \frac{1}{\mathrm{i}\rho\omega} \frac{\partial p(\mathbf{x})}{\partial \mathbf{n}_b} = v_b(\mathbf{x}), \quad \mathbf{x} \in \Gamma, \tag{3}$$

where $\mathbf{n}_b$ is the unit outward normal to the physical boundary at the point $\mathbf{x}$, p_b and v_b are the prescribed pressure and normal velocity at the boundary, respectively, ρ is the medium density and $\mathrm{i} = \sqrt{-1}$. If the geometry of the problem can be considered invariant in the x direction, Eq. (1) can be transformed to the wavenumber domain using a Fourier transform of the form

$$\bar{f}\left(k_x, y, z, \omega\right) = \int_{-\infty}^{+\infty} f\left(x, y, z, \omega\right) \mathrm{e}^{\mathrm{i}k_x x} \mathrm{d}x, \tag{4}$$

where k_x is the wavenumber associated to the longitudinal direction x and f can be the pressure p or the normal velocity v. The bar notation is used to denote that the variable is expressed in the wavenumber domain. This transformation results in the 2.5D version of the system equations, represented by the 2D modified Helmholtz equation

$$\left(\Delta - k_a^2\right) \bar{p}(\mathbf{x}) = 0, \quad \mathbf{x} = (y, z) \in \Omega, \tag{5}$$

where Δ is here the 2D Laplacian operator and $k_a = \sqrt{k_x^2 - k^2}$ is the acoustic wavenumber for the 2.5D domain. The Dirichlet and Neumann boundary conditions can be also transformed to the 2.5D domain, resulting in

$$\bar{p}(\mathbf{x}) = \bar{p}_b(\mathbf{x}), \quad \mathbf{x} = (y, z) \in \Gamma, \tag{6}$$

$$\bar{v}(\mathbf{x}) = \frac{1}{\mathrm{i}\rho\omega} \frac{\partial \bar{p}(\mathbf{x})}{\partial \mathbf{n}} = \bar{v}_b(\mathbf{x}), \quad \mathbf{x} = (y, z) \in \Gamma. \tag{7}$$

2.2. The SBM for 2.5D acoustic problems

The SBM approximates the solution of the problem in a given domain with a linear combination of fundamental solutions of the governing differential equation. To achieve this, the SBM firstly determines a set of virtual sources that complies with the prescribed boundary conditions evaluated in a set of collocation points placed along the boundary Γ. In contrast to the MFS, the collocation and source points of the SBM are placed on the physical boundary, avoiding the need of auxiliary one. In this work, it is also assumed that the set of collocation points is geometrically coincident with the set of virtual sources. This scheme is illustrated in Fig. 1. Virtual sources can be then subsequently used to evaluate the response in the domain. The method employs the OIFs to evaluate the interpolation matrix terms associated to the coincident source–collocation points.

Thus, the SBM approximates the acoustic pressure $\bar{p}$ and particle velocity $\bar{v}$ at a generic point $\mathbf{x}$ considering the effect of N sources located at positions $\mathbf{s}_j$, being $(j = 1, 2, \ldots, N)$, resulting in the expressions

$$\bar{p}(\mathbf{x}) = \sum_{j=1}^{N} \alpha_j \, \bar{G}(\mathbf{x}, \mathbf{s}_j, k_a), \quad \mathbf{x} \in \Omega, \tag{8}$$

$$\mathrm{i}\rho\omega\bar{v}(\mathbf{x}) = \sum_{j=1}^{N} \alpha_j \, \bar{H}(\mathbf{x}, \mathbf{s}_j, k_a, \mathbf{n}_x), \quad \mathbf{x} \in \Omega, \tag{9}$$

where α_j $(j = 1, 2, \ldots, N)$ are the unknown source strengths and

$$\bar{G}(\mathbf{x}, \mathbf{s}, k_a) = \begin{cases} \dfrac{1}{2\pi} K_0(k_a r), & \text{for } k_a \neq 0, \\ G^L(\mathbf{x}, \mathbf{s}), & \text{for } k_a = 0, \end{cases} \tag{10}$$

$$\bar{H}(\mathbf{x}, \mathbf{s}, k_a, \mathbf{n}_x) = \frac{\partial \bar{G}(\mathbf{x}, \mathbf{s}, k_a)}{\partial \mathbf{n}_x} = \begin{cases} -\dfrac{k_a}{2\pi} K_1(k_a r) \dfrac{\partial r}{\partial \mathbf{n}_x}, & \text{for } k_a \neq 0, \\ H^L(\mathbf{x}, \mathbf{s}, \mathbf{n}_x), & \text{for } k_a = 0, \end{cases} \tag{11}$$

are the 2.5D fundamental solutions of the sound pressure and particle velocity, respectively, for the modified Helmholtz equation. K_0 and K_1 are the modified Bessel functions of the second kind of order zero and one, respectively, r is the distance between the source point $\mathbf{s}$ and the arbitrary field point $\mathbf{x}$, $\mathbf{n}_x$ arbitrary unit vector that represents the direction along which the particle velocity is calculated, while $G^L(\mathbf{x}, \mathbf{s})$ and $H^L(\mathbf{x}, \mathbf{s}, \mathbf{n}_x)$ are the fundamental solutions of potential and flux of the 2D Laplace equation, respectively, which take the form

$$G^L(\mathbf{x}, \mathbf{s}) = -\frac{1}{2\pi} \ln(r), \tag{12}$$

$$H^L(\mathbf{x}, \mathbf{s}, \mathbf{n}_x) = \frac{\partial G^L(\mathbf{x}, \mathbf{s})}{\partial \mathbf{n}_x} = -\frac{1}{2\pi r} \frac{\partial r}{\partial \mathbf{n}_x}. \tag{13}$$

Eqs. (8) and (9) can be transformed to evaluate the response at the mth collocation point $\mathbf{s}_m$ as

$$\bar{p}(\mathbf{s}_m) = \alpha_m \bar{G}_{mm} + \sum_{j=1, j\neq m}^{N} \alpha_j \, \bar{G}(\mathbf{s}_m, \mathbf{s}_j, k_a), \quad \mathbf{s}_m \in \Gamma, \tag{14}$$

$$\mathrm{i}\rho\omega\bar{v}(\mathbf{s}_m) = \alpha_m \bar{H}_{mm} + \sum_{j=1, j\neq m}^{N} \alpha_j \, \bar{H}(\mathbf{s}_m, \mathbf{s}_j, k_a, \mathbf{n}_b), \quad \mathbf{s}_m \in \Gamma. \tag{15}$$

where $\bar{G}_{mm}$ and $\bar{H}_{mm}$ are defined as the OIFs of the 2.5D fundamental solutions of Helmholtz equation. Thus, the source strengths for the Dirichlet boundary condition can be obtained by

$$\boldsymbol{\alpha} = \bar{\mathbf{G}}^{-1} \bar{\mathbf{p}}_b, \tag{16}$$

while for the Neumann boundary condition they can be computed as

$$\boldsymbol{\alpha} = \bar{\mathbf{H}}^{-1} \bar{\mathbf{v}}_b, \tag{17}$$

where $\bar{\mathbf{G}}$ and $\bar{\mathbf{H}}$ are the SBM interpolation matrices, being their diagonal terms the previously mentioned OIFs, and where $\boldsymbol{\alpha}$ is a vector that

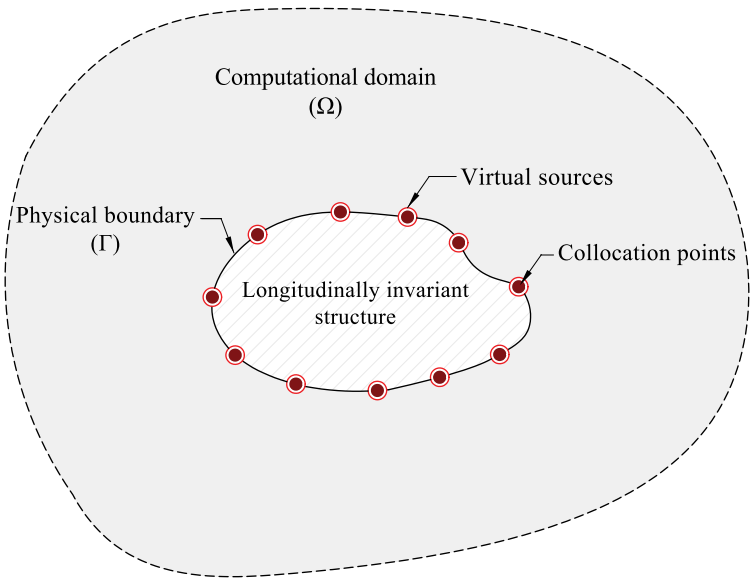

Fig. 1. Schematic sketch of the SBM approach with the adopted sources and collocation points distributions. Red circles denote virtual sources and brown dots represent collocation points. For interpretation of the references to colour in this figure legend, the reader is referred to the web version of this article.

collects all source strengths while $\bar{\mathbf{p}}_b$ and $\bar{\mathbf{v}}_b$ are vectors that collect the imposed boundary conditions evaluated at all collocation points.

Due to the same order of the singularities arising for small source-receiver distances in both fundamental solutions of Laplace and Helmholtz equations, $\bar{G}_{mm}$ and $\bar{H}_{mm}$ can be derived via the asymptotic form of the fundamental solutions of the 2D Laplace equation when the source-receiver distance is small, as

$$\bar{G}_{mm} = \begin{cases} G^L_{mm} + \dfrac{1}{2\pi}\left(-\ln(k_a) + \ln 2 - \gamma\right), & \text{for } k_a \neq 0, \\ G^L_{mm}, & \text{for } k_a = 0, \end{cases} \tag{18}$$

$$\bar{H}_{mm} = H^L_{mm}, \tag{19}$$

where G^L_{mm} and H^L_{mm} are respectively the OIFs of the fundamental solutions of 2D Laplace equation and γ is the Euler constant. The detailed derivations of Eqs. (18) and (19) are given in Appendix. By using the desingularisation provided by the subtracting and adding-back technique, the OIFs for the fundamental solutions of 2D Laplace equation can be derived as [24,26,27]

$$G^L_{mm} = \frac{1}{L_m}\int_{\Gamma_s} G^L(\mathbf{x}_m, \mathbf{s}_j)\,\mathrm{d}\Gamma_s(\mathbf{s}) = -\frac{1}{2\pi}\ln\left(\frac{L_m}{2\pi}\right), \tag{20}$$

$$H^L_{mm} = \frac{1}{L_m}\left(1 - \sum_{j=1, j\neq m}^{N} L_j H^L(\mathbf{x}_m, \mathbf{s}_j, \mathbf{n}_b)\right), \tag{21}$$

where L_j is the half length of the curve between the $(j-1)$th collocation or source point and the $(j+1)$th ones, as shown in Fig. 2. Note that, for the special case when $k_a = 0$, the modified Helmholtz equation reduces to the Laplace equation. Accordingly, the chosen fundamental solutions and OIFs for this particular case should be the ones associated to the Laplace equation.

3. Numerical results and discussions

In this section, a study of the validity and accuracy of the proposed 2.5D SBM is presented. Three benchmark examples are used in this regard: the acoustic radiation and wave scattering problems for an infinite cylinder and the acoustic radiation of an infinite beam with a star-like cross section. In the case of the infinite cylinder, the new method is compared with the available analytical solution as well as three numerical methods: the 2.5D linear-element BEM (2.5D LE-BEM), the 2.5D quadratic-element BEM (2.5D QE-BEM) and the 2.5D MFS

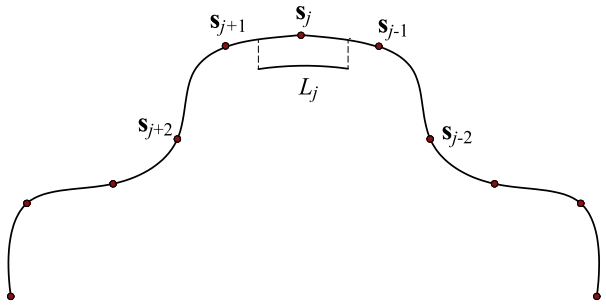

Fig. 2. Schematic configuration of the source points and the corresponding L_j to the jth source. The same configuration applies for the collocation points and the distance L_m.

approaches. In the case of the beam with star-like cross section, only the above-mentioned numerical approaches are considered in the detailed comparison due to the lack of an available analytical solution. Both 2.5D LE-BEM and 2.5D QE-BEM approaches have been constructed based on OpenBEM software presented in [37]. For all three examples, the sound wave speed has been considered to be as $c = 340$ m/s, while the density of the medium adopted is $\rho = 1.225$ kg/m^3.

Along this study, the pressure and velocity at $x = 0$ due to unitary harmonic boundary conditions of the general form $\delta(x)\mathrm{e}^{\mathrm{i}\omega t}$ are used for comparison purposes, which can be computed from the inverse Fourier transform (corresponding to the Fourier transform defined in Eq. (4)) as

$$f_0 = f\,(0, y, z, \omega) = \frac{1}{2\pi}\int_{-\infty}^{+\infty} \bar{f}\left(k_x, y, z, \omega\right)\mathrm{d}k_x, \tag{22}$$

where f can be representing either pressure p or normal velocity v, as before. Moreover, the numerical accuracy is proposed to be globally evaluated in a set of N_t test points by the root mean square error (RMSE) defined as

$$\mathrm{RMSE} = \frac{\sqrt{\frac{1}{N_t}\sum_{k=1}^{N_t}\left|p_{0n}(\mathbf{x}_k) - p_{0r}(\mathbf{x}_k)\right|^2}}{\sqrt{\frac{1}{N_t}\sum_{k=1}^{N_t}\left|p_{0r}(\mathbf{x}_k)\right|^2}}, \tag{23}$$

where $p_{0n}(\mathbf{x}_k)$ and $p_{0r}(\mathbf{x}_k)$ are the numerical and reference solutions at the kth test point, respectively. Depending on the example, reference

solutions are analytical or, in the case of no available analytical solution, they are computed with a highly accurate numerical method. Furthermore, to characterize the error decay rate with the discretization, i.e. the decay rate of the RMSE as a function of the number of collocation points or nodes, for each numerical method and for each specific case study, the following formulation is given:

$$E_d = -\frac{\ln(\varepsilon(N_1)) - \ln(\varepsilon(N_2))}{\ln(N_1) - \ln(N_2)}, \tag{24}$$

where $\varepsilon(N_1)$ and $\varepsilon(N_2)$ are the errors corresponding to each numerical method for N_1 and N_2 collocation points (or nodes, depending on the method), respectively.

For the implementation of the 2.5D MFS, it is also assumed the same number of virtual sources than collocation points. Regarding both boundary element approaches, the amount of Gaussian points adopted for the integration is 8. To implement the 2.5D SBM, two scenarios are considered. In the first one, it is supposed that the 2.5D SBM uses the exact geometrical data from the curve equation of the boundary to determine the influence lengths L_i, used to calculate the OIFs, and to obtain the normal vectors, required for the computation of the 2.5D fundamental solutions. To facilitate the comparisons, this method is called 2.5D SBM-EGD in this paper. In the second scenario, the 2.5D SBM utilizes the nodal geometry data, and it is referred as 2.5D SBM-NGD approach. Hereby, it is assumed that the 2.5D SBM discretizes the boundary to the collocation points by considering a linear shape of the boundary between them. For the 2.5D SBM-NGD approach, the OIFs are calculated numerically considering this approximated boundary.

3.1. Example 1. Radiation problem of an infinite pulsating cylinder

The problem under consideration in this example is the sound field generated by an infinitely long pulsating cylinder. For this case, the analytical solution of the induced pressure field in the wavenumber-frequency domain is [31]

$$p(r, k_a) = \frac{i\rho\omega v_n K_0(k_a r)}{k_a K_1(k_a a)}, \quad r > a, \tag{25}$$

where a is the radius of the cylinder, r is the distance between the evaluation point and the cylinder axis, ρ is the air density, ω is the angular frequency, v_n is the amplitude of the vibration velocity of the cylinder boundary in the radial direction and K_0 and K_1 are the modified Bessel functions of the second kind of order zero and one, respectively. In this simulation, a cylinder of unit radius is considered and a radial pulsating displacement of the form $u_n(t) = \delta(x)e^{i\omega t}$ is considered as a Neumann boundary condition. In this boundary condition, the radial displacement is applied uniformly in all points of the boundary. A $\delta(x)$ distribution of the boundary condition in the longitudinal direction is selected since it is an adequate choice to verify the method for any potential longitudinal distribution of the boundary condition. This comes from the fact that a delta distribution $\delta(x)$ transforms into a constant spectrum in the wavenumber domain, allowing for a verification of the method all along the wavenumber spectrum at once. Regarding the 2.5D MFS, the auxiliary boundary where the virtual sources are uniformly distributed is a concentric circle of radius $a-d$, being d the distance between the physical and auxiliary boundaries.

To obtain the RMSE, two distinct sets of $N_t = 100$ test points are considered, both distributed along the plane $y-z$ on circles centred at the cylinder axis and with radii $r = 1.1$ m and $r = 20$ m, representing the near-field and far-field responses, respectively. For both sets, the test points are uniformly distributed along the circle. Two frequencies are considered for the present RMSE analysis: 100 Hz and 2000 Hz. The pressures p_0 delivered by the different methods at each test point are computed via Eq. (22), in which the numerical integration is carried out by the trapezoidal rule using a logarithmic sampling for the wavenumber with a total amount of 2^8 sampling points ranging between 10^{-3} rad/m and a higher limit, the latter being specifically determined for each frequency. The number of collocation points or nodes per wavelength (referred also as N/λ or nodes/wavelength from now on) is varying in the range of 2–20, where $\lambda = 2\pi c/\omega$. The error decay rates calculated via Eq. (24) are evaluated for two consecutive N/λ in the range of 10–20. The results of the described error analysis comparing the different numerical approaches are illustrated in Fig. 3. Overall, it can be observed that all methods deliver a good accuracy at both near-field and far-field points for the two frequencies selected, and also their associated errors decrease as the number of collocation points or boundary nodes increase. Consequently, it can be stated that all of methods are verified with the analytical solution for this calculation example. It should be also mentioned that for all frequencies below the selected frequency, errors delivered by the methods are always smaller. In Fig. 3, it can be also observed that the 2.5D MFS shows the most accurate solutions among all methods. However, as depicted, the 2.5D MFS solutions are sensitive to the placement of the fictitious boundary and only using the optimal fictitious boundary leads to much higher accuracy for all N/λ values considered. Comparing the results obtained from the 2.5D SBM and the 2.5D BEM, it is found that the 2.5D SBM-NGD presents a higher numerical accuracy than the 2.5D LE-BEM. However, it never reaches the accuracy of the 2.5D QE-BEM. It is also worth to mention that both 2.5D SBM-NGD and 2.5D LE-BEM present the same error decay rates of about $E_d = 2$. On the other hand, the 2.5D SBM-EGD converges rapidly, in this particular case, to the analytical solution showing an error decay rate of about $E_d = 3$. Thus, it can be observed that the 2.5D SBM-EGD shows more accuracy than the 2.5D QE-BEM at the frequency of 100 Hz for $N/\lambda > 16$ and $N/\lambda > 4$ for the near-field and far-field test points, respectively, since 2.5D QE-BEM tends to reach the analytical solution following an error decay rate of $E_d = 1$ for large N/λ. The results obtained indicate how strongly the accuracy of the SBM solutions is affected by the exact or the approximated definitions of the boundary shape. This conclusion is specially relevant to denote the strong effect that the uncertainty of the geometrical definition of the boundary has over the accuracy of the proposed method. This is of special importance in the application of the proposed scheme to real engineering problems, which retain an inherent uncertainty on the parametric definition of boundary geometry.

3.2. Example 2. Wave scattering problem of an infinite cylinder

In this case, the scattering problem of an infinite cylinder subjected to an incident plane wave of the form $\delta(x)e^{ik_y y}e^{i\omega t}$ propagating along the horizontal direction y is considered. The analytical solution of the scattering field is [38]

$$p(r,\theta) = -\frac{J_0'(k_a a)}{H_0'(k_a a)} H_0^{(1)}(k_a r) - 2\sum_{n=1}^{\infty} i^n \frac{J_n'(k_a a)}{H_n'(k_a a)} H_n^{(1)}(k_a r)\cos n\theta, \quad r \geq a, \quad 0 \leq \theta \leq 2\pi, \tag{26}$$

where a is the radius of the cylinder, (r,θ) represents the location of the evaluation point in the polar coordinate system, J_n is the Bessel function of the order n, $H_n^{(1)}$ is the Hankel function of the first kind of order n and the prime denotes their differentiation with respect to its argument. As before, a cylinder of unit radius has been considered. As in the previous example, the analysis is done for the frequencies of 100 Hz and 2000 Hz. The analytical solution is calculated by using 150 terms for the series appearing in Eq. (26), which ensures double precision accuracy.

Fig. 4 displays the results of the RMSE analysis for the wave scattering problem under consideration and for the different numerical methods. The same test points sets presented in the previous example are adopted here. The results illustrate that the 2.5D MFS approach shows the most accurate performance for both frequencies and for both

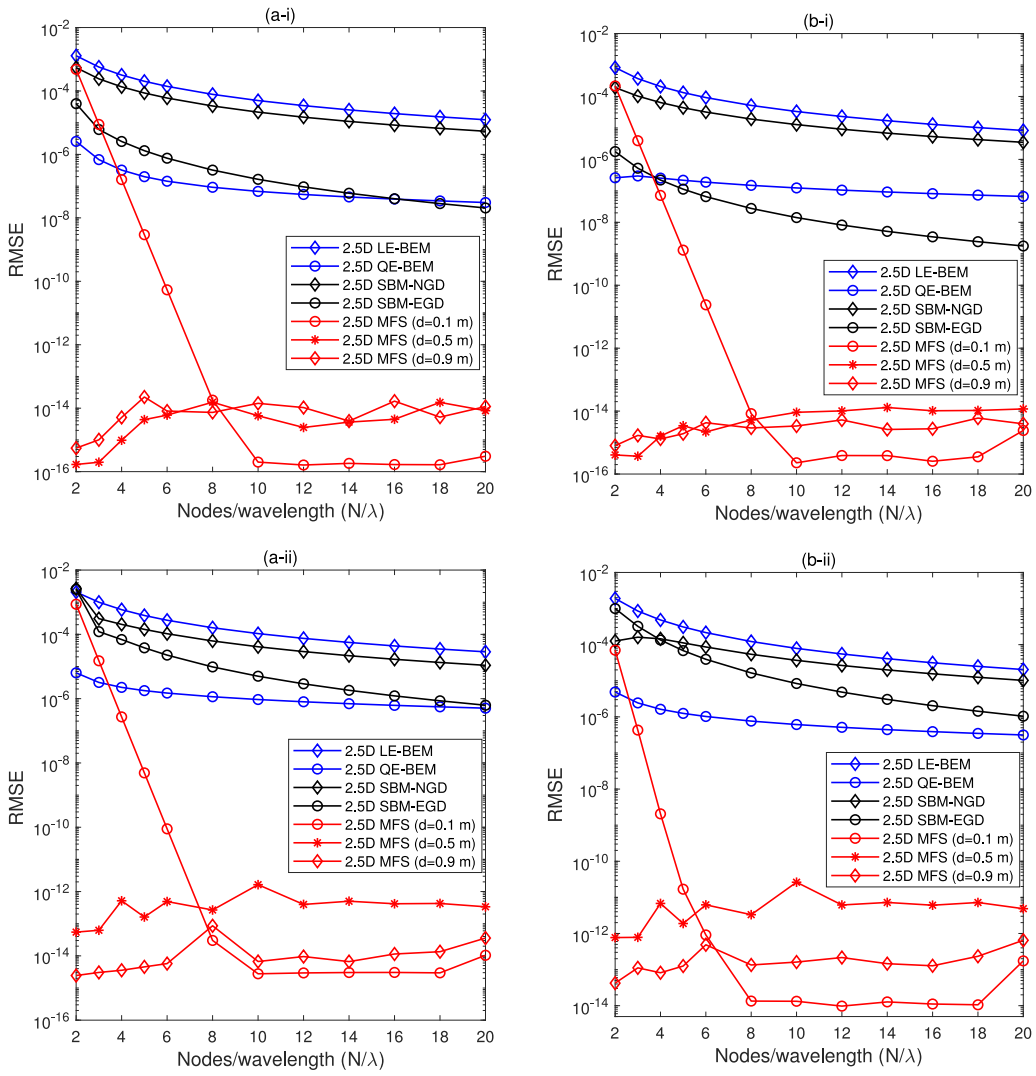

Fig. 3. RMSE analysis of the different methods considered for the radiation problem of an infinite pulsating cylinder obtained at (a) near-field and (b) far-field test points and for the frequencies of (i) 100 Hz and (ii) 2000 Hz. The corresponding upper limits of the wavenumber sampling considered for integration at the frequency of 100 Hz are 10 rad/m and 2 rad/m for near-field and far-field test points, respectively. At the frequency of 2000 Hz, the corresponding higher limits are 60 rad/m and 40 rad/m at near-field and far-field test points, respectively. For interpretation of the references to colour in this figure legend, the reader is referred to the web version of this article.

near-field and far-field situations. However, the method strongly relies on an optimal placement of the fictitious boundary, specially at low N/λ. This behaviour is more significant in this example in comparison to the radiation problem. All the other methods stably converge to the analytical solution by increasing the number of nodes per wavelength. At the frequency of 100 Hz, similar to the conclusion in Example 1, the 2.5D SBM-NGD provides slightly more accurate results than the 2.5D LE-BEM under the same number of boundary nodes per wavelength, following in both cases an error decay rate of $E_d = 2$. For this frequency, these two methods are delivering errors 2–4 orders of magnitude higher than the 2.5D QE-BEM and the 2.5D SBM-EGD, which show similar accuracy levels specially at low N/λ. For this particular problem, the 2.5D QE-BEM shows higher error decay rates than the 2.5D SBM-EGD as the number of nodes per wavelength increase. Specifically, the 2.5D QE-BEM and 2.5D SBM-NGD for this frequency deliver error decay rates of $E_d = 4$ and $E_d = 3$, respectively. On the other hand, at the frequency of 2000 Hz different trends are observed. As the nodes per wavelength increase, the 2.5D SBM-NGD shows a numerical accuracy 1–2 orders of magnitude better than the 2.5D LE-BEM. The error decay rates of these two methods for this situation are similar, being the one associated to the 2.5D SBM-NGD slightly larger. The 2.5D SBM-NGD also delivers more accurate solutions than the 2.5D QE-BEM at $N/\lambda \leq 10$, a behaviour not observed in Example 1, although the error decay rate of the 2.5D QE-BEM to the analytical solution is significantly higher, in this case.

In the two aforementioned examples, the validity and accuracy of the proposed 2.5D SBM were elaborately presented in the framework of the acoustic problems applying on the infinite circular cylinder. Of course, no aspect of the present method is restricted to consideration of simple geometries, such as circle. Hence, in the following, the feasibility of the method to deal with problems under arbitrary geometries is investigated. To demonstrate this, the acoustic radiation problem of an infinite pulsating beam with a constant star-like cross section is designed.

3.3. Example 3. Radiation problem of an infinite pulsating star-like beam

In this example, the problem of the sound field radiated by an infinite pulsating beam with a constant cross section of star-like shape is considered. The star-like shape adopted in this example is shown in Fig. 5a and it is parametrically defined by

$$\rho(\theta) = \frac{1}{m^2}\left[m^2 + 2m + 2 - 2(m+1)\cos(m\theta)\right], \quad y(\theta) = \rho(\theta)\cos\theta, \quad z(\theta) = \rho(\theta)\sin\theta, \tag{27}$$

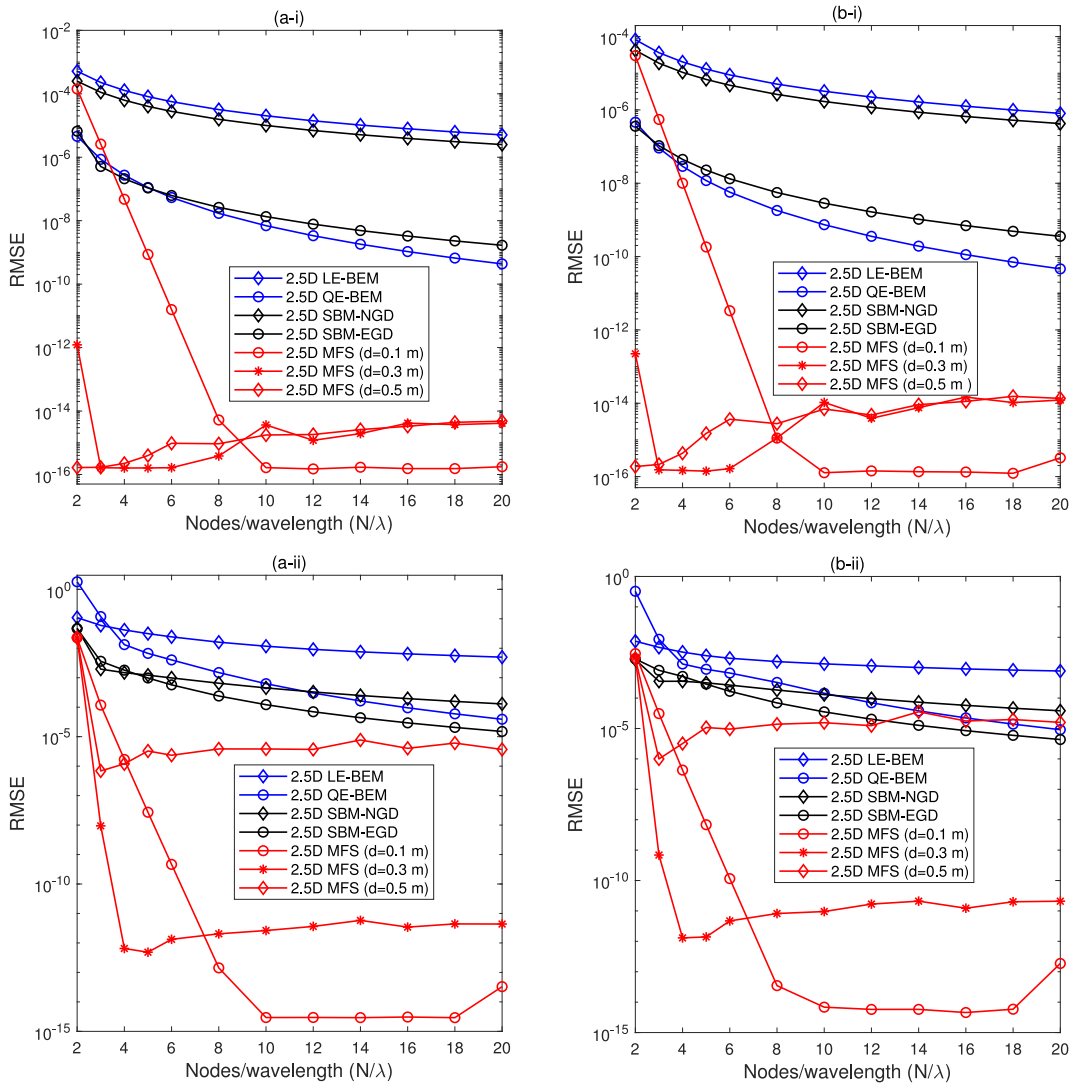

Fig. 4. RMSE analysis of the different methods considered for the scattering problem of an infinite cylinder obtained at (a) near-field and (b) far-field test points and for the frequencies of (i) 100 Hz and (ii) 2000 Hz. The corresponding upper limits of the wavenumber sampling considered for integration are 1.8 rad/m and 36.9 rad/m at the frequencies of 100 Hz and 2000 Hz, respectively, for both sets of near-field and far-field test points. For interpretation of the references to colour in this figure legend, the reader is referred to the web version of this article.

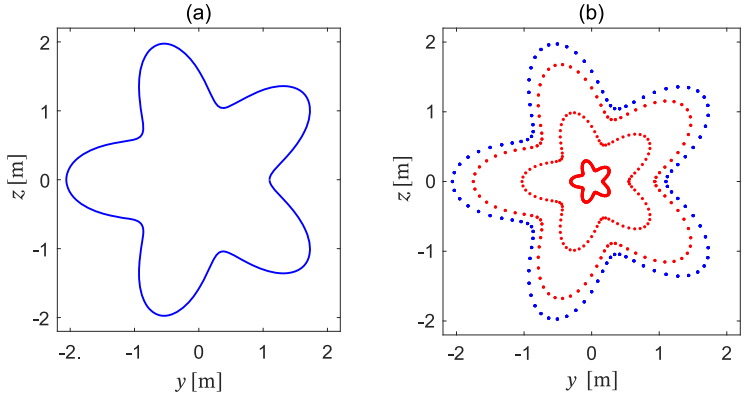

Fig. 5. (a) Star-like shape captured by Eq. (27) with $m = 5$, (b) discretized physical boundary (blue), the fictitious boundary of the 2.5D MFS located with different distance from the physical boundary (red). For interpretation of the references to colour in this figure legend, the reader is referred to the web version of this article.

in which $m = 5$.

Since no analytical solution is available for this problem, the 2.5D QE-BEM is used as alternative reference solution to the analytical one required in Eq. (23). For this aim, the 2.5D QE-BEM is adopted with 40 nodes per wavelength ($N/\lambda = 40$) to ensure that high numerical accuracy is provided by this reference solution. The same boundary

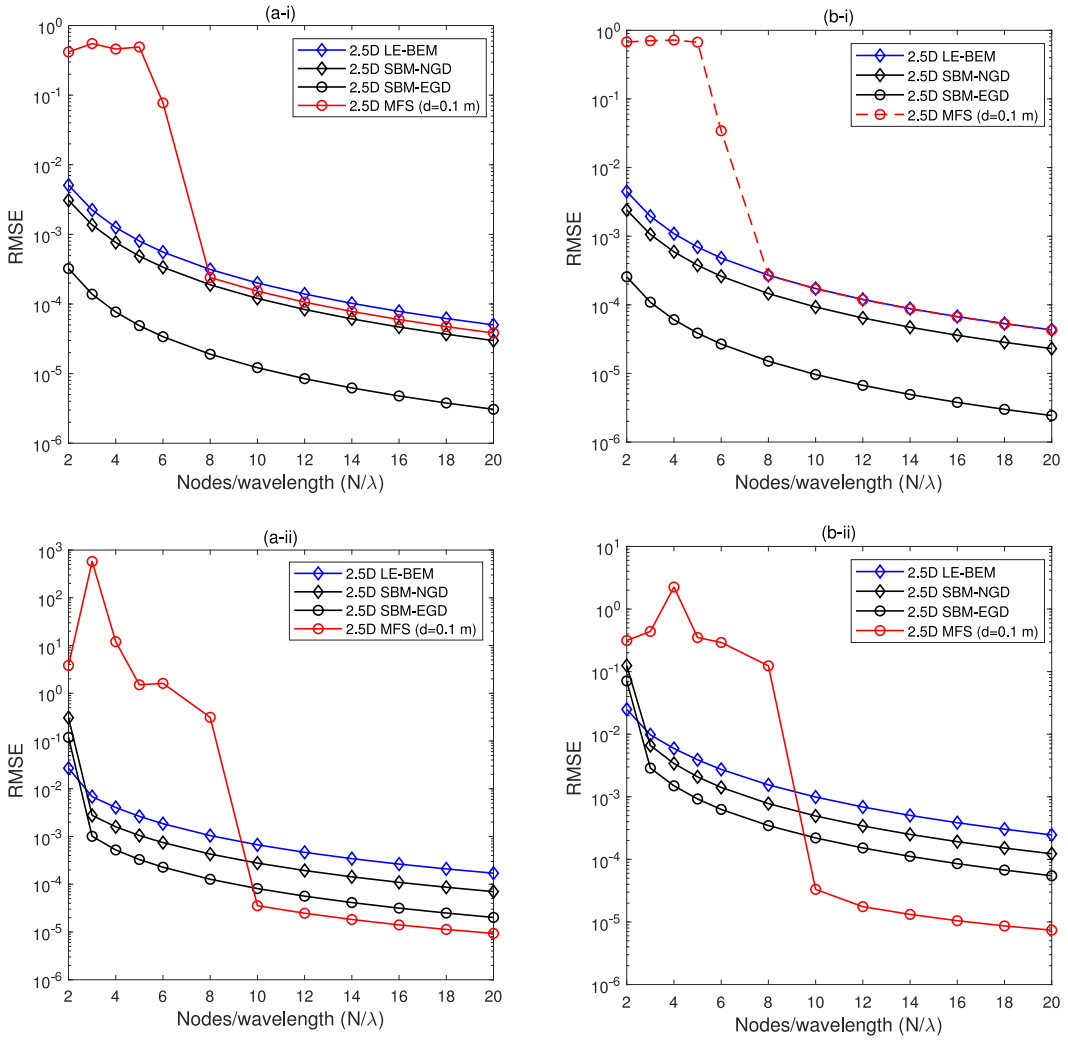

Fig. 6. RMSE analysis of the different methods considered for the radiation problem of an infinite star-like beam obtained at (a) near-field and (b) far-field test points and for the frequencies of (i) 100 Hz and (ii) 2000 Hz. At the frequency of 100 Hz, the corresponding intervals of k_x considered for integration are $[10^{-3}, 5]$ rad/m and $[10^{-3}, 3]$ rad/m for near-field and far-field test points, respectively. At the frequency of 2000 Hz, the corresponding intervals are $[10^{-3}, 50]$ rad/m and $[10^{-3}, 45]$ rad/m, respectively. For interpretation of the references to colour in this figure legend, the reader is referred to the web version of this article.

condition employed in Example 1 is considered here. The computational analysis is carried out for the frequencies of 100 Hz and 2000 Hz. The numerical integration to perform the Fourier transform is here carried out considering a variable lower limit of integration.

Regarding the implementation of the 2.5D SBM-EGD, the influence lengths required in the calculation of the OIFs in Eq. (21), the arc lengths, can be obtained via numerical integration. In order to implement the 2.5D MFS, it is worth to mention that, because of complexity of the geometry in this example, specifying the optimal placement of the fictitious boundary is a perplexing try-error work. Sever numerical instability and ill-conditioning situations can occur if this distance is not selected properly. In the current 2.5D MFS implementation, it is supposed that the fictitious boundary has a star-like shape scaled with respect to the physical one. The geometry of the auxiliary boundary can be parametrically defined by

$$\rho(\theta) = \frac{1-d}{m^2}\left[m^2 + 2m + 2 - 2(m+1)\cos(m\theta)\right], \tag{28}$$

where $1-d$, in this example, refers to the scale factor of the auxiliary boundary geometry. Accordingly, d is the only parameter that defines the virtual sources distribution and the one to be optimized to ensure the highest numerical accuracy of the 2.5D MFS. As shown in Fig. 5b, it is assumed that the virtual sources are forming a uniform angular distribution along the auxiliary boundary. Considering this, an optimization process for d was carried out, leading to an optimal value for d of 0.1 m.

Fig. 6 illustrates the results of the RMSE analysis for Example 3 computed by different numerical methods. In this case, two distinct sets of $N_t = 100$ test points uniformly distributed along the circles with radii of $r = 2.2$ m and $r = 20$ m are adopted, representing the near-field and far-field points, respectively. Overall, it can be found that by increasing nodes density per wavelength at the two frequencies selected, the 2.5D LE-BEM and both 2.5D SBM schemes stably approach to the reference solution, all with the same error decay rate of $E_d = 2$. However, the 2.5D MFS performs different accuracy trends: it gets steadily close to the reference solution with $E_d = 2$ for $N/\lambda \geq 8$ Hz and $N/\lambda \geq 10$ at the frequencies of 100 Hz and 2000 Hz, respectively, while the method shows severe numerical instabilities for nodes per wavelength less than the mentioned values, a behaviour not detected in the previous examples. At the frequency of 100 Hz, in contrast to the previous examples, the 2.5D SBM-EGD provides the most accurate solutions among all methods and it delivers errors 1–2 orders of magnitude less than the 2.5D LE-BEM and the 2.5D SBM-NGD. At this frequency, the 2.5D SBM-NGD provides slightly more accurate results than the 2.5D LE-BEM under the same number of boundary nodes per wavelength, similar to conclusions from the previous examples. At the

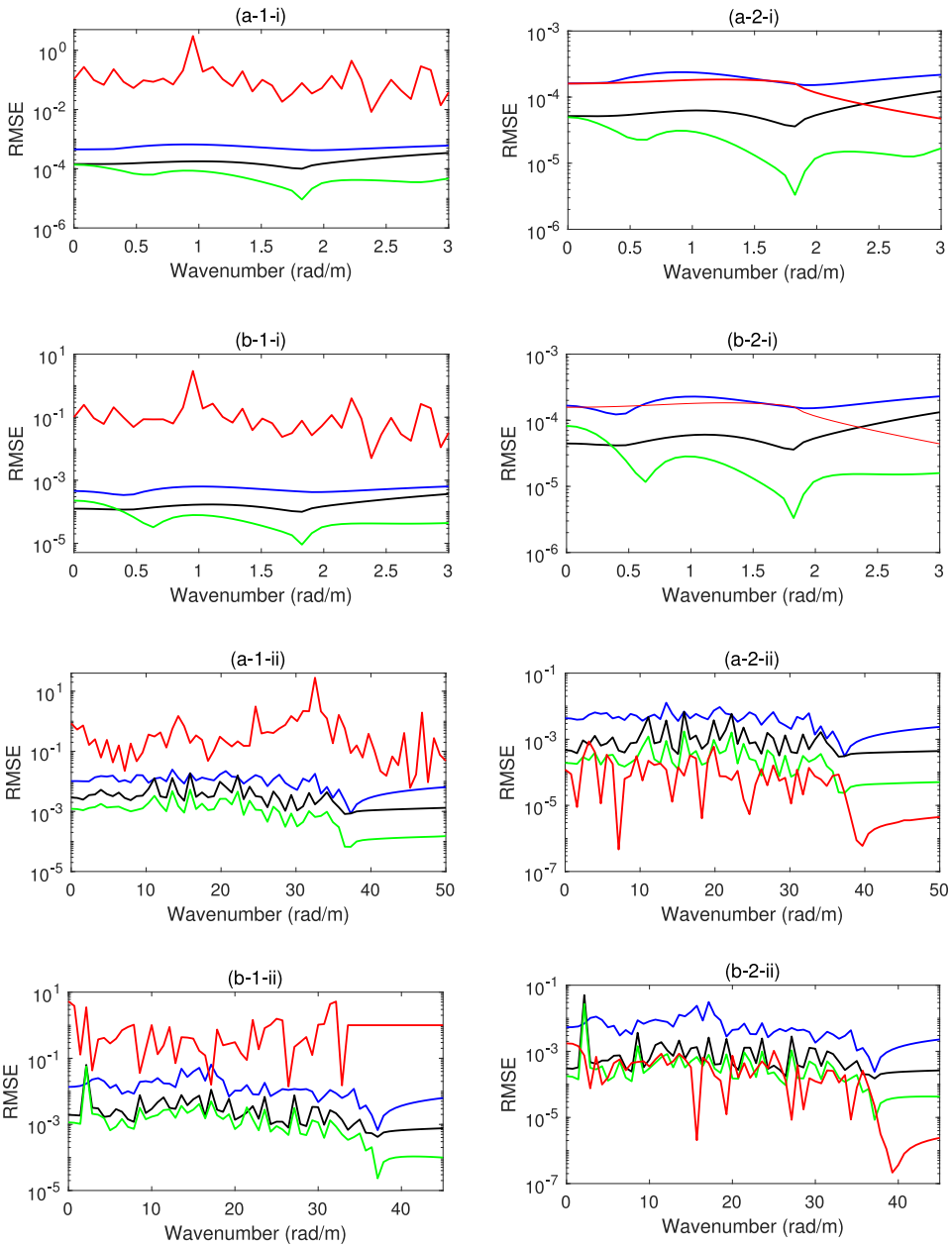

Fig. 7. RMSE analysis for the infinite pulsating star-like beam in the wavenumber domain obtained by the 2.5D SBM-EGD (green line), the 2.5D SBM-NGD (black line), the 2.5D LE-BEM (blue line) and the 2.5D MFS with $d = 0.1$ m (red line) at (a) near-field and (b) far-field test points for (1) $N/\lambda = 6$ and (2) $N/\lambda = 10$ at the frequencies of (i) 100 Hz and (ii) 2000 Hz. For interpretation of the references to colour in this figure legend, the reader is referred to the web version of this article.

frequency of 2000 Hz, except for the results obtained at $N/\lambda = 2$, both 2.5D SBM schemes deliver higher accuracy than 2.5D LE-BEM. However, for $N/\lambda \geq 10$, the most accurate solutions are delivered by the 2.5D MFS, in contrast to the frequency of 100 Hz. However, it is worth to mention that the accuracy of the MFS is largely more sensitive to the location of the virtual boundary than in the previous examples, denoting that an optimization of its location becomes more relevant and more computationally expensive in the case of complex geometries. Consequently, the 2.5D SBM is a more suitable approach for domains with complex boundary geometries in terms of simplicity and robustness.

Here, the error analysis between the methods in the wavenumber domain is also presented for Example 3. This analysis has been carried out in order to evaluate the numerical accuracy of the different 2.5D methods along the wavenumber spectrum and, consequently, to evaluate the validity of using the transfer functions p_0 to robustly compare the accuracy of the methods. In this analysis, the RMSE is reformulated in the wavenumber domain as

$$\text{RMSE} = \frac{\sqrt{\frac{1}{N_t}\sum_{k=1}^{N_t} |\bar{p}_n(\mathbf{x}_k) - \bar{p}_r(\mathbf{x}_k)|^2}}{\sqrt{\frac{1}{N_t}\sum_{k=1}^{N_t} |\bar{p}_r(\mathbf{x}_k)|^2}}, \tag{29}$$

where $\bar{p}_r(\mathbf{x}_k)$ and $\bar{p}_n(\mathbf{x}_k)$ are the pressure responses computed by the reference solution adopted in Example 3 and by the other 2.5D numerical methods at the kth test point, respectively. Fig. 7 shows the results of the mentioned error analysis for $N/\lambda = 6$ and $N/\lambda = 10$. These results are presented only in the wavenumber ranges where the responses have significant spectral content. According to Fig. 7, both 2.5D SBM schemes and the 2.5D LE-BEM are in a close agreement with the 2.5D QE-BEM in the wavenumber domain. Since the error is distributed all along the significant wavenumber range, the employed

transfer functions p_0 are capturing the error properly and it can be concluded that they can be used for the comparison of methods accuracy. Furthermore, it can be observed that, in general, both 2.5D SBM-EGD and 2.5D SBM-NGD provide higher accuracy than the 2.5D LE-BEM for both $N/\lambda = 6$ and $N/\lambda = 10$. In case of the 2.5D MFS, it is observed that the method constructed with 6 nodes per wavelength delivers inaccurate results and shows numerical instability along all the wavenumber domain, a behaviour already demonstrated in previous analysis (Fig. 6). In contrast, when it is implemented with 10 nodes per wavelength, a close agreement with the 2.5D QE-BEM is obtained.

4. Conclusions

In this study, a 2.5D SBM approach for acoustic radiation and scattering problems in the framework of longitudinally infinite and invariant structures is developed. The method determines the OIFs for 2.5D fundamental solutions of the Helmholtz equation by means of the OIFs of fundamental solutions of the Laplace equation taking advantage of the same singularity order in both fundamental solutions. These OIFs are derived by applying a desingularisation procedure based on the subtracting and adding-back technique. The proposed 2.5D SBM has been implemented considering two different calculation scenarios of the influence lengths and unit normals. The first scenario is considering the exact shape equation of the boundary while the second one performs a nodal-based approximation, being these methods referred to the 2.5D SBM-EGD and the 2.5D SBM-NGD, respectively. The feasibility and accuracy of the present schemes are studied through three benchmark examples: the acoustic radiation and wave scattering problems for an infinite cylinder and the acoustic radiation of an infinite beam with a star-like cross section. In order to make a detailed assessment of the proposed 2.5D SBM schemes, the available analytical solutions and other numerical methodologies including the 2.5D MFS and the 2.5D BEM with linear and quadratic elements are employed and compared in terms of numerical accuracy and computational efficiency.

The detailed comparison performed demonstrates the validity and accuracy of the present 2.5D SBM schemes. In the problems related to the infinite cylinder, the error analysis shows that the 2.5D SBM-EGD approaches rapidly to the analytical solution with an error decay rate of $E_d = 3$, while the 2.5D SBM-NGD delivers an error decay rate of $E_d = 2$. As a newfound conclusion, it is indicated that the 2.5D SBM-NGD provides higher numerical accuracy than the 2.5D LE-BEM and lower than the 2.5D QE-BEM, while the 2.5D SBM-EGD can compete in several situations with the levels of accuracy of the 2.5D QE-BEM, being the radiation problem at high frequency the only case where the 2.5D SBM-EGD is not reaching the quadratic BEM performance. It is worth mentioning that, although the 2.5D MFS performs the most accurate results in the circular domain examples, its solutions are highly sensitive to the optimal placement of fictitious boundary, demonstrating the robustness issues of that method with respect to the other ones studied. In the problem of the infinite star-like beam, both 2.5D SBM-EGD and 2.5D SBM-NGD perform with higher accuracy than the 2.5D MFS and the 2.5D LE-BEM at low frequencies, especially the SBM-EGD. The 2.5D MFS shows severe numerical instabilities depending on the placement of the fictitious boundary at low and moderate amounts of nodes per wavelength. It should be highlighted that the numerical accuracy of the 2.5D SBM solutions is intensely affected by the exact or approximated definitions of the boundary shape. The results obtained depict that using the approximated nodal data of the boundary instead of its exact one leads to a significant reduction in the accuracy and convergence of the 2.5D SBM. This is of special importance for the application of the proposed scheme to real engineering problems in where the arbitrary shape of the boundary avoids determining an exact analytical expression of its geometry.

In terms of computational efficiency, the present 2.5D SBM schemes inherits various advantages with respect to former methods. Due to its meshless nature, the proposed 2.5D SBM scheme performs more efficiently than equivalent 2.5D BEM approaches thanks to avoiding two procedures: the construction of a boundary mesh and the sophisticated numerical integration over the singularities that BEM approaches normally carry out. Furthermore, the method is found to be more robust than the 2.5D MFS, since it does not need to deal with the troublesome placement of the fictitious boundary which is revealed to be a complex and time-consuming procedure especially in the case of irregular boundary geometries.

Overall, the 2.5D SBM is an accurate and computationally fast numerical method and it appears to be a competitive alternative to other available 2.5D numerical methods for acoustic analysis.

Declaration of competing interest

The authors declare that they have no known competing financial interests or personal relationships that could have appeared to influence the work reported in this paper.

Acknowledgements

This research has been carried out with the financial support of the project VIBWAY: Fast computational tool for railway-induced vibrations and re-radiated noise assessment, with reference RTI2018-096819-B-I00, supported by the Ministerio de Ciencia e Innovación, Retos de Investigación 2018. Also, the first author would like to thank the financial support provided by the FPI-UPC 2017 grant (reference 07), funded by the Universitat Politècnica de Catalunya (UPC) and the Banco Santander. This work has been also financially supported by the Project PTDC/ECI-EGC/3352/2021, funded by FEDER funds through COMPETE2020 - Programa Operacional Competitividade e Internacionalização (POCI) and by national funds (PIDDAC) through FCT/MCTES.

Appendix. OIFs for the 2.5D fundamental solutions of the modified Helmholtz equation

In this appendix, the 2.5D OIFs associated to the modified Helmholtz equation are derived. Adopting the subtracting and adding-back technique on Eq. (9) when collocation points are placed on the boundary results in

$$\begin{aligned}\mathrm{i}\rho\omega\bar{v}(\mathbf{s}_m) = \sum_{j=1}^{N}\alpha_j\bar{H}(\mathbf{s}_m,\mathbf{s}_j,k_a,\mathbf{n}_b) &= \sum_{j=1}^{N}(\alpha_j-\alpha_m\Pi_{jm})\bar{H}(\mathbf{s}_m,\mathbf{s}_j,k_a,\mathbf{n}_b)\\ &+\alpha_m\sum_{j=1}^{N}\Pi_{jm}\Big(\bar{H}(\mathbf{s}_m,\mathbf{s}_j,k_a,\mathbf{n}_b)-H^L(\mathbf{s}_m,\mathbf{s}_j,\mathbf{n}_b)\Big)\\ &+\alpha_m\sum_{j=1}^{N}\Pi_{jm}\Big(H^L(\mathbf{s}_m,\mathbf{s}_j,\mathbf{n}_b)+H_I^L(\mathbf{s}_m,\mathbf{s}_j,\mathbf{n}_b)\Big)\\ &-\alpha_m\sum_{j=1}^{N}\Pi_{jm}H_I^L(\mathbf{s}_m,\mathbf{s}_j,\mathbf{n}_b),\end{aligned} \tag{A.1}$$

where $H_I^L(\mathbf{s}_m,\mathbf{s}_j,\mathbf{n}_b)$ denotes the fundamental solutions of the flux for the Laplace equation in interior problems and where $\Pi_{jm} = L_j/L_m$, noting that $\Pi_{mm} = 1$. According to the dependency of the outward normal vectors on the fundamental solutions of interior and exterior problems for the Laplace equation, the following identities can be stated:

$$\begin{aligned}H^L(\mathbf{s}_m,\mathbf{s}_j,\mathbf{n}_b) &= -H_I^L(\mathbf{s}_m,\mathbf{s}_j,\mathbf{n}_b), \quad \text{for } \mathbf{s}_m \neq \mathbf{s}_j,\\ H^L(\mathbf{s}_m,\mathbf{s}_j,\mathbf{n}_b) &= H_I^L(\mathbf{s}_m,\mathbf{s}_j,\mathbf{n}_b), \quad \text{for } \mathbf{s}_m = \mathbf{s}_j.\end{aligned} \tag{A.2}$$

Furthermore, another important identity reads as

$$\lim_{\mathbf{s}_j\to\mathbf{s}_m}\left(\frac{\partial G^L(\mathbf{s}_m,\mathbf{s}_j)}{\partial\mathbf{n}_{b_m}}+\frac{\partial G^L(\mathbf{s}_m,\mathbf{s}_j)}{\partial\mathbf{n}_{b_j}}\right)=0, \tag{A.3}$$

for which if the boundary is a straight line, the above equation is explicitly equal to zero, since $\mathbf{n}_{b_m} = \mathbf{n}_b(\mathbf{s}_m)$ is equal to $\mathbf{n}_{b_j} = \mathbf{n}_b(\mathbf{s}_j)$ at all points. For problems with arbitrarily smooth geometries, fundamental solutions as well as normal vectors smoothly approach to their corresponding ones when source ($\mathbf{s}_j$) and collocation ($\mathbf{s}_m$) points get closer to each other along a line segment. In those situations, Eq. (A.3) is valid. Considering the relationship between the fundamental solutions of the Laplace and Helmholtz equations for small source–receiver distances as follows

$$\bar{H}(\mathbf{s}_m, \mathbf{s}_j, k_a, \mathbf{n}_b) = H^L(\mathbf{s}_m, \mathbf{s}_j, \mathbf{n}_b), \quad r \to 0, \tag{A.4}$$

and also using the help of Eqs. (A.2) and (A.3), Eq. (A.1) can be regularized as:

$$\begin{aligned} \mathrm{i}\rho\omega\bar{v}(\mathbf{s}_m) = & \sum_{j=1,j\neq m}^{N} (\alpha_j - \alpha_m \Pi_{jm}) \bar{H}(\mathbf{s}_m, \mathbf{s}_j, k_a, \mathbf{n}_b) \\ & + \alpha_m \sum_{j=1,j\neq m}^{N} \Pi_{jm} \left(\bar{H}(\mathbf{s}_m, \mathbf{s}_j, k_a, \mathbf{n}_b) - H^L(\mathbf{s}_m, \mathbf{s}_j, \mathbf{n}_b) \right) \\ & + \alpha_m \sum_{j=1,j\neq m}^{N} \Pi_{jm} \left(H^L(\mathbf{s}_m, \mathbf{s}_j, \mathbf{n}_b) + H_I^L(\mathbf{s}_m, \mathbf{s}_j, \mathbf{n}_b) \right) \\ & - \alpha_m \sum_{j=1}^{N} \Pi_{jm} H_I^L(\mathbf{s}_m, \mathbf{s}_j, \mathbf{n}_b). \end{aligned} \tag{A.5}$$

Now, the above equation is regularized except for its last term which still involves singularity. However, it has a finite value equal to $V_m = -1/L_m$, which can be derived based on the following direct boundary integral equation:

$$u(\mathbf{x}_m) = \int_\Gamma \left(G_I^L(\mathbf{x}_m, \mathbf{s}) \frac{\partial u(\mathbf{s})}{\partial \mathbf{n}_b} - u(\mathbf{s}) H_I^L(\mathbf{x}_m, \mathbf{s}, \mathbf{n}_b) \right) \mathrm{d}\Gamma(\mathbf{s}), \quad \mathbf{x}_m \in \Omega_I. \tag{A.6}$$

Substituting the simple test solution $u(\mathbf{s}) = 1$ and $\partial u(\mathbf{s})/\partial \mathbf{n}_b = 0$, into Eq. (A.6) we can obtain the following equation:

$$\int_\Gamma H_I^L(\mathbf{x}_m, \mathbf{s}, \mathbf{n}_b) \mathrm{d}\Gamma(\mathbf{s}) = -1, \quad \mathbf{x}_m \in \Omega_I. \tag{A.7}$$

When the field point $\mathbf{x}_m$ approaches the boundary, we can discretize Eq. (A.7) as follows:

$$\begin{aligned} \int_\Gamma H_I^L(\mathbf{x}_m, \mathbf{s}, \mathbf{n}_b) \mathrm{d}\Gamma(\mathbf{s}) &= \sum_{j=1}^{N} \int_{\Gamma_j} H_I^L(\mathbf{x}_m, \mathbf{s}, \mathbf{n}_b) \mathrm{d}\Gamma_j(\mathbf{s}) \\ &\approx \sum_{j=1}^{N} H_I^L(\mathbf{x}_m, \mathbf{s}_j, \mathbf{n}_b) L_j = -1, \quad \mathbf{x}_m \in \Gamma. \end{aligned} \tag{A.8}$$

Dividing by non-zero value L_m, we have

$$\sum_{j=1}^{N} \Pi_{jm} H_I^L(\mathbf{x}_m, \mathbf{s}_j, \mathbf{n}_b) = V_m, \quad \mathbf{x}_m \in \Gamma, \tag{A.9}$$

where $V_m = -1/L_m$. Then, the regular formulation of Eq. (A.1) is represented as:

$$\begin{aligned} \mathrm{i}\rho\omega\bar{v}(\mathbf{s}_m) &= \sum_{j=1,j\neq m}^{N} \alpha_j \bar{H}(\mathbf{s}_m, \mathbf{s}_j, k_a, \mathbf{n}_b) + \alpha_m \sum_{j=1,j\neq m}^{N} \Pi_{jm} H_I^L(\mathbf{s}_m, \mathbf{s}_j, \mathbf{n}_b) - \alpha_m V_m \\ &= \sum_{j=1,j\neq m}^{N} \alpha_j \bar{H}(\mathbf{s}_m, \mathbf{s}_j, k_a, \mathbf{n}_b) - \alpha_m \sum_{j=1,j\neq m}^{N} \Pi_{jm} H^L(\mathbf{s}_m, \mathbf{s}_j, \mathbf{n}_b) - \alpha_m V_m. \end{aligned} \tag{A.10}$$

Compared with Eq. (15) at $\mathbf{s}_m = \mathbf{s}_j$, it is obtained that:

$$\bar{H}_{mm} = H_{mm}^L = -V_m - \sum_{j=1,j\neq m}^{N} \Pi_{jm} H^L(\mathbf{s}_m, \mathbf{s}_j, \mathbf{n}_b), \tag{A.11}$$

which is the OIFs of the 2.5D fundamental solutions of Helmholtz equation for Neumann boundary conditions in Eq. (15).

Thanks to the following asymptotic expression between the Helmholtz and Laplace fundamental solutions:

$$\bar{G}(\mathbf{s}_m, \mathbf{s}_j, k_a) = G^L(\mathbf{s}_m, \mathbf{s}_j) + \frac{1}{2\pi} \left(-\ln(k_a) + \ln 2 - \gamma \right), \quad r \to 0 \tag{A.12}$$

the OIFs $\bar{G}_{mm}$ of the 2.5D fundamental solutions of Helmholtz equation in Eq. (14) can be determined indirectly by calculating the OIFs G_{mm}^L of the Laplace equation, namely,

$$\bar{G}_{mm} = G_{mm}^L + \frac{1}{2\pi} \left(-\ln(k_a) + \ln 2 - \gamma \right), \tag{A.13}$$

where the OIFs G_{mm}^L can be derived as [24,27]:

$$G_{mm}^L = \frac{1}{L_m} \int_{\Gamma_s} G^L(\mathbf{x}_m, \mathbf{s}) \mathrm{d}\Gamma_s(\mathbf{s}) = -\frac{1}{2\pi} \ln\left(\frac{L_m}{2\pi} \right). \tag{A.14}$$

References

[1] Harari I. A survey of finite element methods for time-harmonic acoustics. Comput Meth Appl Mech Eng 2006;195(13–16):1594–607. http://dx.doi.org/10.1016/j.cma.2005.05.030.

[2] Liu Y. On the BEM for acoustic wave problems. Eng Anal Boundary Elem 2019;107(March):53–62. http://dx.doi.org/10.1016/j.enganabound.2019.07.002.

[3] Shippy DJ, Kondapalli PS, Fairweather G. Analysis of acoustic scattering in fluids and solids by the method of fundamental solutions. Math Computr Modell 1990;14(C):74–9. http://dx.doi.org/10.1016/0895-7177(90)90150-L.

[4] Kondapalli PS, Shippy DJ, Fairweather G. Analysis of acoustic scattering in fluids and solids by the method of fundamental solutions. J Acoust Soc Am 1992;91(4):1844–54. http://dx.doi.org/10.1121/1.403714.

[5] Karageorghis A. The method of fundamental solutions for the calculation of the eigenvalues of the Helmholtz equation. Appl Math Lett 2001;14:837–42. http://dx.doi.org/10.1016/S0893-9659(01)00053-2.

[6] Fairweather G, Karageorghis A, Martin PA. The method of fundamental solutions for scattering and radiation problems. Eng Anal Boundary Elem 2003;27(7):759–69. http://dx.doi.org/10.1016/S0955-7997(03)00017-1.

[7] Marin L. Treatment of singularities in the method of fundamental solutions for two-dimensional Helmholtz-type equations. Appl Math Model 2010;34(6):1615–33. http://dx.doi.org/10.1016/j.apm.2009.09.009, URL http://dx.doi.org/10.1016/j.apm.2009.09.009.

[8] Karageorghis A, Lesnic D, Marin L. The MFS for the identification of a sound-soft interior acoustic scatterer. Eng Anal Boundary Elem 2017;83(January):107–12. http://dx.doi.org/10.1016/j.enganabound.2017.07.021, URL http://dx.doi.org/10.1016/j.enganabound.2017.07.021.

[9] Qu W, Fan CM, Gu Y. Localized method of fundamental solutions for interior Helmholtz problems with high wave number. Eng Anal Boundary Elem 2019;107(June):25–32. http://dx.doi.org/10.1016/j.enganabound.2019.06.018.

[10] Costa EGdA, Godinho LMC, Santiago JAF, Mansur WJ, Peters FC. Application of the method of fundamental solutions to predict the acoustic performance of T-shaped thin barriers. Eng Anal Bound Elem 2019;99(November 2018):142–56. http://dx.doi.org/10.1016/j.enganabound.2018.11.009.

[11] Chen JT, Chang MH, Chen KH, Lin SR. The boundary collocation method with meshless concept for acoustic eigenanalysis of two-dimensional cavities using radial basis function. J Sound Vib 2002;257(4):667–711. http://dx.doi.org/10.1006/jsvi.2002.5038.

[12] Chen W, Hon YC. Numerical investigation on convergence of boundary knot method in the analysis of homogeneous Helmholtz, modified Helmholtz, and convection-diffusion problems. Comput Meth Appl Mech Eng 2003;192(15):1859–75. http://dx.doi.org/10.1016/S0045-7825(03)00216-0.

[13] Wang F, Gu Y, Qu W, Zhang C. Localized boundary knot method and its application to large-scale acoustic problems. Comput Meth Appl Mech Eng 2020;361:112729. http://dx.doi.org/10.1016/j.cma.2019.112729.

[14] Yue X, Wang F, Zhang C, Zhang H. Localized boundary knot method for 3D inhomogeneous acoustic problems with complicated geometry. App Math Modell 2021;92:410–21. http://dx.doi.org/10.1016/j.apm.2020.11.022.

[15] Young DL, Chen KH, Lee CW. Singular meshless method using double layer potentials for exterior acoustics. J Acoust Soc Am 2006;119(1):96–107. http://dx.doi.org/10.1121/1.2141130.

[16] Liu L. Single layer regularized meshless method for three dimensional exterior acoustic problem. Eng Ana Boundary Elem 2017;77(February):138–44. http://dx.doi.org/10.1016/j.enganabound.2017.02.001.

[17] Chen W, Wang FZ. A method of fundamental solutions without fictitious boundary. Eng Anal Bound Elem 2010;34(5):530–2. http://dx.doi.org/10.1016/j.enganabound.2009.12.002.

[18] Lin J, Chen W, Chen CS. Numerical treatment of acoustic problems with boundary singularities by the singular boundary method. J Sound Vib 2014;333(14):3177–88. http://dx.doi.org/10.1016/j.jsv.2014.02.032.

[19] Fu ZJ, Chen W, Gu Y. Burton-Miller-type singular boundary method for acoustic radiation and scattering. J Sound Vib 2014;333(16):3776–93. http://dx.doi.org/10.1016/j.jsv.2014.04.025.

[20] Fu ZJ, Chen W, Lin J, Cheng AH. Singular boundary method for various exterior wave applications. Int J Comput Methods 2015;12(2):1–16. http://dx.doi.org/10.1142/S0219876215500115.

[21] Qu W, Chen W, Gu Y. Fast multipole accelerated singular boundary method for the 3D Helmholtz equation in low frequency regime. Comput Math Appl 2015;70(4):679–90. http://dx.doi.org/10.1016/j.camwa.2015.05.017.

[22] Qu W, Chen W, Zheng C. Diagonal form fast multipole singular boundary method applied to the solution of high-frequency acoustic radiation and scattering. Int J Numer Methods Eng 2017;111(9):803–15. http://dx.doi.org/10.1002/nme.5478.

[23] Li W. A fast singular boundary method for 3D Helmholtz equation. Comput Math Appl 2019;77(2):525–35. http://dx.doi.org/10.1016/j.camwa.2018.09.055.

[24] Fu Z, Chen W, Wen P, Zhang C. Singular boundary method for wave propagation analysis in periodic structures. J Sound Vib 2018;425:170–88. http://dx.doi.org/10.1016/j.jsv.2018.04.005.

[25] Wang F, Chen Z, Li P-w, Fan C-m. Localized singular boundary method for solving Laplace and Helmholtz equations in arbitrary 2D domains. Eng Anal Boundary Elem 2021;129(April):82–92. http://dx.doi.org/10.1016/j.enganabound.2021.04.020.

[26] Chen W, Gu Y. Recent advances on singular boundary method. Joint Int. Workshop Trefftz Method 2011;4(5):543–58. http://dx.doi.org/10.4208/aamm.11-m11118.

[27] Fu Z, Chen W, Chen J, Qu W. Singular boundary method: Three regularization approaches and ExteriorWave applications. CMES -Comput Model Eng Sci 2014;100(1):59–84. http://dx.doi.org/10.3970/cmes.2014.099.255.

[28] Li J, Chen W, Fu Z, Sun L. Explicit empirical formula evaluating original intensity factors of singular boundary method for potential and Helmholtz problems. Eng Anal Boundary Elem 2016;73(May):161–9. http://dx.doi.org/10.1016/j.enganabound.2016.10.003.

[29] Li J, Fu Z, Chen W, Qin QH. A regularized approach evaluating origin intensity factor of singular boundary method for Helmholtz equation with high wavenumbers. Eng Anal Boundary Elem 2019;101(January):165–72. http://dx.doi.org/10.1016/j.enganabound.2019.01.008.

[30] Sheng X, Jones CJC, Thompson DJ. Prediction of ground vibration from trains using the wavenumber finite and boundary element methods. J Sound Vib 2006;293(3–5):575–86. http://dx.doi.org/10.1016/j.jsv.2005.08.040.

[31] Sheng X, Zhong T, Li Y. Vibration and sound radiation of slab high-speed railway tracks subject to a moving harmonic load. J Sound Vib 2017;395:160–86. http://dx.doi.org/10.1016/j.jsv.2017.02.024.

[32] Li H, Thompson D, Squicciarini G, Liu X, Rissmann M, Denia FD, Giner-Navarro J. Using a 2.5D boundary element model to predict the sound distribution on train external surfaces due to rolling noise. J Sound Vib 2020;486:115599. http://dx.doi.org/10.1016/j.jsv.2020.115599.

[33] Deng T, Sheng X, Jeong H, Thompson DJ. A two-and-half dimensional finite element/boundary element model for predicting the vibro-acoustic behaviour of panels with poro-elastic media. J Sound Vib 2021;505:116147. http://dx.doi.org/10.1016/j.jsv.2021.116147.

[34] Ghangale D, Colaço A, Alves Costa P, Arcos R. A methodology based on structural finite element method-boundary element method and acoustic boundary element method models in 2.5D for the prediction of reradiated noise in railway-induced ground-borne vibration problems. J Vib Acoust 2019;141(June):31011. http://dx.doi.org/10.1115/1.4042518.

[35] Costa PA, Amado-mendes P. Prediction of vibrations and reradiated noise due to railway traffic : A comprehensive hybrid model based on a finite element method and method of fundamental solutions approach. J Vib Acoustic 2017;139(December):1–10. http://dx.doi.org/10.1115/1.4036929.

[36] Wei X, Luo W. 2.5D Singular boundary method for acoustic wave propagation. Appl Math Lett 2021;112:106760. http://dx.doi.org/10.1016/j.aml.2020.106760.

[37] Henríquez VC, Juhl PM. OpenBEM–an open source boundary element method software in acoustics. In: Proceedings of Internoise. Lisbon, Portugal; 2010.

[38] Perrey-Debain E, Trevelyan J, Bettess P. Plane wave interpolation in direct collocation boundary element method for radiation and wave scattering: numerical aspects and applications. J Sound Vib 2003;261(5):839–58. http://dx.doi.org/10.1016/S0022-460X(02)01006-4.